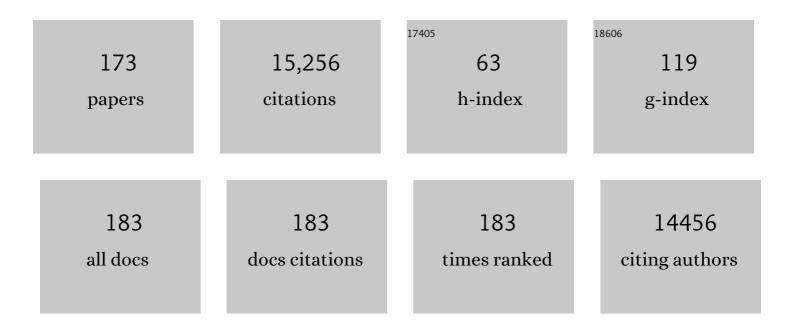
Curtis Berlinguette

List of Publications by Year in descending order

Source: https://exaly.com/author-pdf/897644/publications.pdf Version: 2024-02-01



#	Article	IF	CITATIONS
1	Gas diffusion electrodes and membranes for CO2 reduction electrolysers. Nature Reviews Materials, 2022, 7, 55-64.	23.3	265
2	Selective hydrogenation of furfural using a membrane reactor. Energy and Environmental Science, 2022, 15, 215-224.	15.6	37
3	Porous metal electrodes enable efficient electrolysis of carbon capture solutions. Energy and Environmental Science, 2022, 15, 705-713.	15.6	61
4	Quantification of the Effect of an External Magnetic Field on Water Oxidation with Cobalt Oxide Anodes. Journal of the American Chemical Society, 2022, 144, 733-739.	6.6	20
5	Continuum Model to Define the Chemistry and Mass Transfer in a Bicarbonate Electrolyzer. ACS Energy Letters, 2022, 7, 834-842.	8.8	39
6	A self-driving laboratory advances the Pareto front for material properties. Nature Communications, 2022, 13, 995.	5.8	55
7	Electrocatalysts Derived from Copper Complexes Transform CO into C ₂₊ Products Effectively in a Flow Cell. Chemistry - A European Journal, 2022, 28, e202200340.	1.7	10
8	Electrolytic conversion of carbon capture solutions containing carbonic anhydrase. Journal of Inorganic Biochemistry, 2022, 231, 111782.	1.5	13
9	Flexible automation accelerates materials discovery. Nature Materials, 2022, 21, 722-726.	13.3	33
10	Electrolytic Methane Production from Reactive Carbon Solutions. ACS Energy Letters, 2022, 7, 1712-1718.	8.8	23
11	A magnetic twist on CO2 electrolysis. Trends in Chemistry, 2022, 4, 465-466.	4.4	0
12	Conversion of Reactive Carbon Solutions into CO at Low Voltage and High Carbon Efficiency. ACS Central Science, 2022, 8, 749-755.	5.3	32
13	Ring walking as a regioselectivity control element in Pd-catalyzed C-N cross-coupling. Nature Communications, 2022, 13, .	5.8	11
14	A self-driving laboratory designed to accelerate the discovery of adhesive materials. , 2022, 1, 382-389.		14
15	Permeability Matters When Reducing CO ₂ in an Electrochemical Flow Cell. ACS Energy Letters, 2022, 7, 2382-2387.	8.8	15
16	Designing anion exchange membranes for CO2 electrolysers. Nature Energy, 2021, 6, 339-348.	19.8	209
17	Electrolysis Can Be Used to Resolve Hydrogenation Pathways at Palladium Surfaces in a Membrane Reactor. Jacs Au, 2021, 1, 336-343.	3.6	11
18	Physical Separation of H ₂ Activation from Hydrogenation Chemistry Reveals the Specific Role of Secondary Metal Catalysts. Angewandte Chemie - International Edition, 2021, 60, 11937-11942.	7.2	18

#	Article	IF	CITATIONS
19	Physical Separation of H 2 Activation from Hydrogenation Chemistry Reveals the Specific Role of Secondary Metal Catalysts. Angewandte Chemie, 2021, 133, 12044-12049.	1.6	0
20	Impact of Alkali Cation Identity on the Conversion of HCO ₃ ^{â^'} to CO in Bicarbonate Electrolyzers. ChemElectroChem, 2021, 8, 2094-2100.	1.7	29
21	How Catalyst Dispersion Solvents Affect CO ₂ Electrolyzer Gas Diffusion Electrodes. Energy & Fuels, 2021, 35, 19178-19184.	2.5	20
22	An industrial perspective on catalysts for low-temperature CO2 electrolysis. Nature Nanotechnology, 2021, 16, 118-128.	15.6	255
23	A machine vision tool for facilitating the optimization of large-area perovskite photovoltaics. Npj Computational Materials, 2021, 7, .	3.5	11
24	Voltage Matters When Reducing CO ₂ in an Electrochemical Flow Cell. ACS Energy Letters, 2020, 5, 215-220.	8.8	123
25	Hydrogenation without H2 Using a Palladium Membrane Flow Cell. Cell Reports Physical Science, 2020, 1, 100105.	2.8	28
26	Quantification of water transport in a CO ₂ electrolyzer. Energy and Environmental Science, 2020, 13, 5126-5134.	15.6	86
27	Sulfuric Acid Electrolyte Impacts Palladium Chemistry at Reductive Potentials. Chemistry of Materials, 2020, 32, 9098-9106.	3.2	5
28	Bioinspiration in light harvesting and catalysis. Nature Reviews Materials, 2020, 5, 828-846.	23.3	136
29	Electrolytic deuteration of unsaturated bonds without using D2. Nature Catalysis, 2020, 3, 719-726.	16.1	71
30	Quantifying defects in thin films using machine vision. Npj Computational Materials, 2020, 6, .	3.5	18
31	Conversion of Bicarbonate to Formate in an Electrochemical Flow Reactor. ACS Energy Letters, 2020, 5, 2624-2630.	8.8	84
32	pH Matters When Reducing CO ₂ in an Electrochemical Flow Cell. ACS Energy Letters, 2020, 5, 3101-3107.	8.8	131
33	Linking gas diffusion electrode composition to CO ₂ reduction in a flow cell. Journal of Materials Chemistry A, 2020, 8, 19493-19501.	5.2	54
34	Photoelectrochemical Decomposition of Lignin Model Compound on a BiVO ₄ Photoanode. ChemSusChem, 2020, 13, 3622-3626.	3.6	17
35	Strain Influences the Hydrogen Evolution Activity and Absorption Capacity of Palladium. Angewandte Chemie, 2020, 132, 12290-12296.	1.6	9
36	Self-driving laboratory for accelerated discovery of thin-film materials. Science Advances, 2020, 6, eaaz8867.	4.7	306

#	Article	IF	CITATIONS
37	Electrodes Designed for Converting Bicarbonate into CO. ACS Energy Letters, 2020, 5, 2165-2173.	8.8	90
38	Rhenium Complexes of Pyridyl-Mesoionic Carbenes: Photochemical Properties and Electrocatalytic CO ₂ Reduction. Inorganic Chemistry, 2020, 59, 4215-4227.	1.9	43
39	Ï€ covalency in the halogen bond. Nature Communications, 2020, 11, 3310.	5.8	52
40	Molecular Catalysts Boost the Rate of Electrolytic CO ₂ Reduction. ACS Energy Letters, 2020, 5, 1512-1518.	8.8	52
41	Strain Influences the Hydrogen Evolution Activity and Absorption Capacity of Palladium. Angewandte Chemie - International Edition, 2020, 59, 12192-12198.	7.2	28
42	Managing Hydration at the Cathode Enables Efficient CO ₂ Electrolysis at Commercially Relevant Current Densities. ACS Energy Letters, 2020, 5, 1612-1618.	8.8	111
43	Defining Direct Orbital Pathways for Intermolecular Electron Transfer Using Sensitized Semiconducting Surfaces. Inorganic Chemistry, 2020, 59, 14696-14705.	1.9	2
44	Chapter 10. Electrochemical Reactors. RSC Energy and Environment Series, 2020, , 408-432.	0.2	1
45	CO2 electrochemical catalytic reduction with a highly active cobalt phthalocyanine. Nature Communications, 2019, 10, 3602.	5.8	307
46	Design rules for high mobility xanthene-based hole transport materials. Chemical Science, 2019, 10, 8360-8366.	3.7	20
47	Molecular electrocatalysts can mediate fast, selective CO ₂ reduction in a flow cell. Science, 2019, 365, 367-369.	6.0	601
48	Ligands Affect Hydrogen Absorption and Desorption by Palladium Nanoparticles. Chemistry of Materials, 2019, 31, 8679-8684.	3.2	18
49	Analytical electrolyzer enabling operando characterization of flow plates. Review of Scientific Instruments, 2019, 90, 074103.	0.6	5
50	Protocol for Quantifying the Doping of Organic Hole-Transport Materials. ACS Energy Letters, 2019, 4, 2547-2551.	8.8	23
51	Entropic Barriers Determine Adiabatic Electron Transfer Equilibrium. Journal of Physical Chemistry C, 2019, 123, 3416-3425.	1.5	8
52	Revisiting the cold case of cold fusion. Nature, 2019, 570, 45-51.	13.7	48
53	Electrolytic Conversion of Bicarbonate into CO in a Flow Cell. Joule, 2019, 3, 1487-1497.	11.7	177
54	Calorimetry under non-ideal conditions using system identification. Journal of Thermal Analysis and Calorimetry, 2019, 138, 3139-3157.	2.0	2

#	Article	IF	CITATIONS
55	Efficient Electrocatalytic Hydrogenation with a Palladium Membrane Reactor. Journal of the American Chemical Society, 2019, 141, 7815-7821.	6.6	90
56	Facets and vertices regulate hydrogen uptake and release in palladium nanocrystals. Nature Materials, 2019, 18, 454-458.	13.3	96
57	Strain Engineering Electrocatalysts for Selective CO ₂ Reduction. ACS Energy Letters, 2019, 4, 980-986.	8.8	115
58	Supported palladium membrane reactor architecture for electrocatalytic hydrogenation. Journal of Materials Chemistry A, 2019, 7, 26586-26595.	5.2	26
59	Dopant-free molecular hole transport material that mediates a 20% power conversion efficiency in a perovskite solar cell. Energy and Environmental Science, 2019, 12, 3502-3507.	15.6	90
60	Kinetic phases of Ag–Cu alloy films are accessible through photodeposition. Journal of Materials Chemistry A, 2019, 7, 711-715.	5.2	12
61	Spinâ€coated epoxy resin embedding technique enables facile SEM/FIB thickness determination of porous metal oxide ultraâ€thin films. Journal of Microscopy, 2018, 270, 302-308.	0.8	6
62	Tracking precursor degradation during the photo-induced formation of amorphous metal oxide films. Journal of Materials Chemistry A, 2018, 6, 4544-4549.	5.2	6
63	Photodeposited Amorphous Oxide Films for Electrochromic Windows. CheM, 2018, 4, 821-832.	5.8	95
64	Electrolysis of Gaseous CO ₂ to CO in a Flow Cell with a Bipolar Membrane. ACS Energy Letters, 2018, 3, 149-154.	8.8	265
65	Electrolytic CO ₂ Reduction in a Flow Cell. Accounts of Chemical Research, 2018, 51, 910-918.	7.6	735
66	Electrocatalytic Alloys for CO ₂ Reduction. ChemSusChem, 2018, 11, 48-57.	3.6	249
67	Stabilizing Copper for CO ₂ Reduction in Low-Grade Electrolyte. Inorganic Chemistry, 2018, 57, 14624-14631.	1.9	21
68	Resolving orbital pathways for intermolecular electron transfer. Nature Communications, 2018, 9, 4916.	5.8	19
69	Solution-Deposited Solid-State Electrochromic Windows. IScience, 2018, 10, 80-86.	1.9	36
70	Precise Control of Thermal and Redox Properties of Organic Holeâ€Transport Materials. Angewandte Chemie - International Edition, 2018, 57, 15529-15533.	7.2	41
71	Precise Control of Thermal and Redox Properties of Organic Holeâ€Transport Materials. Angewandte Chemie, 2018, 130, 15755-15759.	1.6	15
72	Kinetics teach that electronic coupling lowers the free-energy change that accompanies electron transfer. Proceedings of the National Academy of Sciences of the United States of America, 2018, 115, 7248-7253.	3.3	28

#	Article	IF	CITATIONS
73	Correlating cobalt redox couples to photovoltage in the dye-sensitized solar cell. Dalton Transactions, 2018, 47, 11942-11952.	1.6	21
74	Optical Intramolecular Electron Transfer in Opposite Directions through the Same Bridge That Follows Different Pathways. Journal of the American Chemical Society, 2018, 140, 7176-7186.	6.6	27
75	Accurate Coulometric Quantification of Hydrogen Absorption in Palladium Nanoparticles and Thin Films. Chemistry of Materials, 2018, 30, 3963-3970.	3.2	27
76	Complete electron economy by pairing electrolysis with hydrogenation. Nature Catalysis, 2018, 1, 501-507.	16.1	148
77	Organic chemistry at anodes and photoanodes. Sustainable Energy and Fuels, 2018, 2, 1905-1927.	2.5	76
78	Highâ€Throughput Synthesis of Mixedâ€Metal Electrocatalysts for CO ₂ Reduction. Angewandte Chemie - International Edition, 2017, 56, 6068-6072.	7.2	131
79	On how electron density affects the redox stability of phenothiazine sensitizers on semiconducting surfaces. Chemical Communications, 2017, 53, 2547-2550.	2.2	8
80	High-Voltage Dye-Sensitized Solar Cells Mediated by [Co(2,2′-bipyrimidine) ₃] ^{<i>z</i>} . Inorganic Chemistry, 2017, 56, 2383-2386.	1.9	12
81	Comparative analysis of triarylamine and phenothiazine sensitizer donor units in dye-sensitized solar cells. Chemical Communications, 2017, 53, 2367-2370.	2.2	25
82	Highâ€Throughput Synthesis of Mixedâ€Metal Electrocatalysts for CO ₂ Reduction. Angewandte Chemie, 2017, 129, 6164-6168.	1.6	28
83	Frontispiece: Highâ€Throughput Synthesis of Mixedâ€Metal Electrocatalysts for CO ₂ Reduction. Angewandte Chemie - International Edition, 2017, 56, .	7.2	1
84	On the Electrolytic Stability of Iron-Nickel Oxides. CheM, 2017, 2, 590-597.	5.8	104
85	Photodeposited ruthenium dioxide films for oxygen evolution reaction electrocatalysis. Journal of Materials Chemistry A, 2017, 5, 1575-1580.	5.2	24
86	Rapid Quantification of Film Thickness and Metal Loading for Electrocatalytic Metal Oxide Films. Chemistry of Materials, 2017, 29, 7272-7277.	3.2	11
87	High-temperature high-pressure calorimeter for studying gram-scale heterogeneous chemical reactions. Review of Scientific Instruments, 2017, 88, 084101.	0.6	5
88	Frontispiz: Highâ€Throughput Synthesis of Mixedâ€Metal Electrocatalysts for CO ₂ Reduction. Angewandte Chemie, 2017, 129, .	1.6	0
89	Water Oxidation Catalysis: Tuning the Electrocatalytic Properties of Amorphous Lanthanum Cobaltite through Calcium Doping. ACS Catalysis, 2017, 7, 6385-6391.	5.5	18
90	Brass and Bronze as Effective CO ₂ Reduction Electrocatalysts. Angewandte Chemie, 2017, 129, 16806-16809.	1.6	15

#	Article	IF	CITATIONS
91	Photodecomposition of Metal Nitrate and Chloride Compounds Yields Amorphous Metal Oxide Films. Journal of the American Chemical Society, 2017, 139, 18174-18177.	6.6	17
92	Brass and Bronze as Effective CO ₂ Reduction Electrocatalysts. Angewandte Chemie - International Edition, 2017, 56, 16579-16582.	7.2	43
93	Electrolytic CO ₂ Reduction in Tandem with Oxidative Organic Chemistry. ACS Central Science, 2017, 3, 778-783.	5.3	93
94	Spectroscopic detection of halogen bonding resolves dye regeneration in the dye-sensitized solar cell. Nature Communications, 2017, 8, 1761.	5.8	35
95	Photoelectrochemical oxidation of organic substrates in organic media. Nature Communications, 2017, 8, 390.	5.8	123
96	Evidence for Interfacial Halogen Bonding. Angewandte Chemie, 2016, 128, 6060-6064.	1.6	11
97	Evidence for Interfacial Halogen Bonding. Angewandte Chemie - International Edition, 2016, 55, 5956-5960.	7.2	40
98	Curing BiVO ₄ Photoanodes with Ultraviolet Light Enhances Photoelectrocatalysis. Angewandte Chemie, 2016, 128, 1801-1804.	1.6	94
99	Rapid prototyping of electrolyzer flow field plates. Energy and Environmental Science, 2016, 9, 3417-3423.	15.6	49
100	On How Experimental Conditions Affect the Electrochemical Response of Disordered Nickel Oxyhydroxide Films. Chemistry of Materials, 2016, 28, 5635-5642.	3.2	22
101	Halogen Bonding Promotes Higher Dye-Sensitized Solar Cell Photovoltages. Journal of the American Chemical Society, 2016, 138, 10406-10409.	6.6	65
102	Exposure of WO ₃ Photoanodes to Ultraviolet Light Enhances Photoelectrochemical Water Oxidation. ACS Applied Materials & Interfaces, 2016, 8, 25010-25013.	4.0	26
103	Electrolysis of CO ₂ to Syngas in Bipolar Membrane-Based Electrochemical Cells. ACS Energy Letters, 2016, 1, 1149-1153.	8.8	235
104	Curing BiVO ₄ Photoanodes with Ultraviolet Light Enhances Photoelectrocatalysis. Angewandte Chemie - International Edition, 2016, 55, 1769-1772.	7.2	138
105	Kinetic pathway for interfacial electron transfer from a semiconductor to a molecule. Nature Chemistry, 2016, 8, 853-859.	6.6	96
106	Water oxidation catalysis: an amorphous quaternary Ba-Sr-Co-Fe oxide as a promising electrocatalyst for the oxygen-evolution reaction. Chemical Communications, 2016, 52, 1513-1516.	2.2	63
107	Accounting for the Dynamic Oxidative Behavior of Nickel Anodes. Journal of the American Chemical Society, 2016, 138, 1561-1567.	6.6	91
108	Near-infrared–driven decomposition of metal precursors yields amorphous electrocatalytic films. Science Advances, 2015, 1, e1400215.	4.7	48

#	Article	IF	CITATIONS
109	How a [Co ^{IV} \${^{underline{}}}\$O] ²⁺ Fragment Oxidizes Water: Involvement of a Biradicaloid [Co ^{II} –(â <oâ<)]<sup>2+ Species in Forming the Oï£;O Bo ChemSusChem, 2015, 8, 844-852.</oâ<)]<sup>	ond3.6	46
110	Mapping the performance of amorphous ternary metal oxide water oxidation catalysts containing aluminium. Journal of Materials Chemistry A, 2015, 3, 756-761.	5.2	48
111	Structural Characteristics and Eutaxy in the Photo-Deposited Amorphous Iron Oxide Oxygen Evolution Catalyst. Chemistry of Materials, 2015, 27, 3462-3470.	3.2	28
112	Editorial for the ACS Select Virtual Issue on Inorganic Chemistry Driving the Energy Sciences. Inorganic Chemistry, 2015, 54, 3079-3083.	1.9	5
113	Trisâ€Heteroleptic Ruthenium–Dipyrrinate Chromophores in a Dyeâ€Sensitized Solar Cell. Chemistry - A European Journal, 2015, 21, 2173-2181.	1.7	23
114	Substitution Effects on the Water Oxidation of Ruthenium Catalysts: A Quantum-Chemical Look. Journal of Physical Chemistry C, 2015, 119, 242-250.	1.5	15
115	Water Oxidation Catalysis: Survey of Amorphous Binary Metal Oxide Films Containing Lanthanum and Late 3d Transition Metals. European Journal of Inorganic Chemistry, 2014, 2014, 660-664.	1.0	17
116	Near-IR Photoresponse of Ruthenium Dipyrrinate Terpyridine Sensitizers in the Dye-Sensitized Solar Cells. Inorganic Chemistry, 2014, 53, 5417-5419.	1.9	37
117	Novel triphenylamine-modified ruthenium(ii) terpyridine complexes for nickel oxide-based cathodic dye-sensitized solar cells. RSC Advances, 2014, 4, 5782.	1.7	37
118	Direct Spectroscopic Evidence for Constituent Heteroatoms Enhancing Charge Recombination at a TiO ₂ â^²Ruthenium Dye Interface. Journal of Physical Chemistry C, 2014, 118, 17079-17089.	1.5	20
119	Physicochemical Analysis of Ruthenium(II) Sensitizers of 1,2,3-Triazole-Derived Mesoionic Carbene and Cyclometalating Ligands. Inorganic Chemistry, 2014, 53, 2083-2095.	1.9	81
120	Intramolecular and Lateral Intermolecular Hole Transfer at the Sensitized TiO ₂ Interface. Journal of the American Chemical Society, 2014, 136, 1034-1046.	6.6	54
121	Facile Photochemical Preparation of Amorphous Iridium Oxide Films for Water Oxidation Catalysis. Chemistry of Materials, 2014, 26, 1654-1659.	3.2	201
122	A Heteroleptic Bis(tridentate) Ruthenium(II) Platform Featuring an Anionic 1,2,3-Triazolate-Based Ligand for Application in the Dye-Sensitized Solar Cell. Inorganic Chemistry, 2014, 53, 1637-1645.	1.9	65
123	Donor–π–acceptor organic hybrid TiO2 interfaces for solar energy conversion. Thin Solid Films, 2014, 560, 49-54.	0.8	7
124	Water Oxidation Catalysis: Electrocatalytic Response to Metal Stoichiometry in Amorphous Metal Oxide Films Containing Iron, Cobalt, and Nickel. Journal of the American Chemical Society, 2013, 135, 11580-11586.	6.6	817
125	Cyclometalated Ruthenium(II) Complexes Featuring Tridentate Clickâ€Derived Ligands for Dyeâ€Sensitized Solar Cell Applications. Chemistry - A European Journal, 2013, 19, 14171-14180.	1.7	35
126	Stabilization of Ruthenium Sensitizers to TiO ₂ Surfaces through Cooperative Anchoring Groups. Journal of the American Chemical Society, 2013, 135, 1692-1695.	6.6	123

#	Article	IF	CITATIONS
127	Proton-coupled electron transfer at a [Co-OHx]zunit in aqueous media: evidence for a concerted mechanism. Chemical Science, 2013, 4, 734-738.	3.7	19
128	Homogeneous water oxidation catalysts containing a single metal site. Chemical Communications, 2013, 49, 218-227.	2.2	184
129	Atomic Level Resolution of Dye Regeneration in the Dye-Sensitized Solar Cell. Journal of the American Chemical Society, 2013, 135, 1961-1971.	6.6	133
130	Ruthenium(II) Complexes Bearing a Naphthalimide Fragment: A Modular Dye Platform for the Dye-Sensitized Solar Cell. Inorganic Chemistry, 2013, 52, 3001-3006.	1.9	47
131	Photochemical Route for Accessing Amorphous Metal Oxide Materials for Water Oxidation Catalysis. Science, 2013, 340, 60-63.	6.0	1,321
132	Interrogation of electrocatalytic water oxidation mediated by a cobalt complex. Chemical Communications, 2012, 48, 2107.	2.2	127
133	Cycloruthenated sensitizers: improving the dye-sensitized solar cell with classical inorganic chemistry principles. Dalton Transactions, 2012, 41, 7814.	1.6	101
134	Cyclometalated ruthenium chromophores for the dye-sensitized solar cell. Coordination Chemistry Reviews, 2012, 256, 1438-1450.	9.5	275
135	Bis(tridentate) Ruthenium–Terpyridine Complexes Featuring Microsecond Excited-State Lifetimes. Journal of the American Chemical Society, 2012, 134, 12354-12357.	6.6	206
136	Derivatization of Bichromic Cyclometalated Ru(II) Complexes with Hydrophobic Substituents. Inorganic Chemistry, 2012, 51, 1501-1507.	1.9	25
137	Intramolecular Hole Transfer at Sensitized TiO ₂ Interfaces. Journal of the American Chemical Society, 2012, 134, 8352-8355.	6.6	40
138	Ru complexes of thienyl-functionalized dipyrrins as NCS-free sensitizers for the dye-sensitized solar cell. Chemical Communications, 2012, 48, 8790.	2.2	41
139	Three is not a crowd: efficient sensitization of TiO2 by a bulky trichromic trisheteroleptic cycloruthenated dye. Chemical Communications, 2012, 48, 5599.	2.2	35
140	Systematic Modulation of a Bichromic Cyclometalated Ruthenium(II) Scaffold Bearing a Redox-Active Triphenylamine Constituent. Inorganic Chemistry, 2011, 50, 6019-6028.	1.9	59
141	Electrochemical evidence for catalytic water oxidation mediated by a high-valent cobalt complex. Chemical Communications, 2011, 47, 4249.	2.2	343
142	Regioselective C–H Activation of Cyclometalated Bis-Tridentate Ruthenium Complexes. Organometallics, 2011, 30, 6628-6635.	1.1	10
143	Unraveling the Roles of the Acid Medium, Experimental Probes, and Terminal Oxidant, (NH ₄) ₂ [Ce(NO ₃) ₆], in the Study of a Homogeneous Water Oxidation Catalyst. Inorganic Chemistry, 2011, 50, 3662-3672.	1.9	107
144	External-Stimuli Responsive Photophysics and Liquid Crystal Properties of Self-Assembled "Phosphole-Lipids― Journal of the American Chemical Society, 2011, 133, 17014-17026.	6.6	146

#	Article	IF	CITATIONS
145	Design and Development of Functionalized Cyclometalated Ruthenium Chromophores for Light-Harvesting Applications. Inorganic Chemistry, 2011, 50, 5494-5508.	1.9	180
146	Strategies for Optimizing the Performance of Cyclometalated Ruthenium Sensitizers for Dye‧ensitized Solar Cells. European Journal of Inorganic Chemistry, 2011, 2011, 1806-1814.	1.0	84
147	A Trisheteroleptic Cyclometalated Ru ^{II} Sensitizer that Enables High Power Output in a Dye‧ensitized Solar Cell. Angewandte Chemie - International Edition, 2011, 50, 10682-10685.	7.2	127
148	Inside Cover: A Trisheteroleptic Cyclometalated Ru ^{II} Sensitizer that Enables High Power Output in a Dye‧ensitized Solar Cell (Angew. Chem. Int. Ed. 45/2011). Angewandte Chemie - International Edition, 2011, 50, 10464-10464.	7.2	4
149	Structure–property relationships of acylated asymmetric dithienophospholes. Comptes Rendus Chimie, 2010, 13, 971-979.	0.2	11
150	Examination of Water Oxidation by Catalysts Containing Cofacial Metal Sites. European Journal of Inorganic Chemistry, 2010, 2010, 3135-3142.	1.0	36
151	Electronic Modification of the [Ru ^{II} (tpy)(bpy)(OH ₂)] ²⁺ Scaffold: Effects on Catalytic Water Oxidation. Journal of the American Chemical Society, 2010, 132, 16094-16106.	6.6	299
152	Insight into Water Oxidation by Mononuclear Polypyridyl Ru Catalysts. Inorganic Chemistry, 2010, 49, 2202-2209.	1.9	256
153	Cyclometalated Ru Complexes of Type [Ru ^{II} (<i>N^{â^\$}N</i>) ₂ (<i>C^{â^\$}N</i>)] ^{<i>z</i>} : Physicochemical Response to Substituents Installed on the Anionic Ligand. Inorganic Chemistry, 2010, 49. 4960-4971.	1.9	127
154	Sol–gel synthesis of linear Sn-doped TiO ₂ nanostructures. Journal of Materials Chemistry, 2010, 20, 498-503.	6.7	50
155	Triphenylamine-Modified Ruthenium(II) Terpyridine Complexes: Enhancement of Light Absorption by Conjugated Bridging Motifs. Inorganic Chemistry, 2010, 49, 5335-5337.	1.9	61
156	Solution growth of anatase TiO2 nanowires from transparent conducting glass substrates. Journal of Materials Chemistry, 2010, 20, 5063.	6.7	55
157	Trigonal-Bipyramidal Metal Cyanide Complexes: A Versatile Platform for the Systematic Assessment of the Magnetic Properties of Prussian Blue Materials. Inorganic Chemistry, 2009, 48, 3438-3452.	1.9	78
158	A comparison of several nanoscale photocatalysts in the degradation of a common pollutant using LEDs and conventional UV light. Water Research, 2009, 43, 4499-4506.	5.3	56
159	On the Viability of Cyclometalated Ru(II) Complexes for Light-Harvesting Applications. Inorganic Chemistry, 2009, 48, 9631-9643.	1.9	224
160	Systematic Manipulation of the Light-Harvesting Properties for Tridentate Cyclometalated Ruthenium(II) Complexes. Inorganic Chemistry, 2009, 48, 9644-9652.	1.9	90
161	Simple Protocol for Generating TiO2 Nanofibers in Organic Media. Chemistry of Materials, 2008, 20, 7022-7030.	3.2	52
162	Stabilization of Reduced Molybdenumâ ``Ironâ ``Sulfur Single- and Double-Cubane Clusters by Cyanide Ligation. Inorganic Chemistry, 2007, 46, 510-516.	1.9	28

#	Article	IF	CITATIONS
163	Precursors to Clusters with the Topology of the PNCluster of Nitrogenase:Â Edge-Bridged Double Cubane Clusters [(Tp)2Mo2Fe6S8L4]z:Â Synthesis, Structures, and Electron Transfer Series. Inorganic Chemistry, 2006, 45, 1997-2007.	1.9	37
164	Edge-Bridged Mo2Fe6S8to PN-Type Mo2Fe6S9Cluster Conversion:Â Structural Fate of the Attacking Sulfide/Selenide Nucleophile. Journal of the American Chemical Society, 2006, 128, 11993-12000.	6.6	43
165	Initial synthesis and structure of an all-ferrous analogue of the fully reduced [Fe4S4]0 cluster of the nitrogenase iron protein. Proceedings of the National Academy of Sciences of the United States of America, 2005, 102, 9741-9744.	3.3	70
166	Synthesis of MFe3S4Clusters Containing a Planar MIISite (M = Ni, Pd, Pt), a Structural Element in the C-Cluster of Carbon Monoxide Dehydrogenase. Journal of the American Chemical Society, 2005, 127, 11092-11101.	6.6	38
167	A Charge-Transfer-Induced Spin Transition in a Discrete Complex:Â The Role of Extrinsic Factors in Stabilizing Three Electronic Isomeric Forms of a Cyanide-Bridged Co/Fe Cluster. Journal of the American Chemical Society, 2005, 127, 6766-6779.	6.6	156
168	A Charge-Transfer-Induced Spin Transition in the Discrete Cyanide-Bridged Complex {[Co(tmphen)2]3[Fe(CN)6]2}. Journal of the American Chemical Society, 2004, 126, 6222-6223.	6.6	200
169	Structural Characterization, Magnetic Properties, and Electrospray Mass Spectrometry of Two Jahnâ^'Teller Isomers of the Single-Molecule Magnet [Mn12O12(CF3COO)16(H2O)4]. Inorganic Chemistry, 2004, 43, 1359-1369.	1.9	51
170	Role of the Orbitally Degenerate Mn(III) Ions in the Single-Molecule Magnet Behavior of the Cyanide Cluster {[MnII(tmphen)2]3[MnIII(CN)6]2} (tmphen = 3,4,7,8-tetramethyl-1,10-phenanthroline). Journal of the American Chemical Society, 2004, 126, 16860-16867.	6.6	78
171	Synthesis, Characterization, and Physical Properties of Two Trinuclear, Mixed-Valence Species of Type [1¼3-OMnIIMnIII2(O2CCF3)6(R)3] (R=H2O, CH3COOH). Journal of Cluster Science, 2003, 14, 235-252.	1.7	15
172	Recognition of Topological Isomerism:  Synthesis, Structure, and Magnetic Properties of Two Pentanuclear High-Spin Molecules of the Type [Nill(N-N)2]3[Felll(CN)6]2. Inorganic Chemistry, 2003, 42, 3416-3422.	1.9	65
173	Structural diversity of cyanide-bridged bimetallic clusters based on hexacyanometallate building blocks. Comptes Rendus Chimie, 2002, 5, 665-672.	0.2	15